ADVANCED MATERIALS

www.advmat.de

A Self-Powered and Flexible Organometallic Halide Perovskite Photodetector with Very High Detectivity

*Siu-Fung Leung, Kang-Ting Ho, Po-Kai Kung, Vincent K. S. Hsiao, Husam N. Alshareef, Zhong Lin Wang, and Jr-Hau He**

Flexible and self-powered photodetectors (PDs) are highly desirable for applications in image sensing, smart building, and optical communications. In this paper, a self-powered and flexible PD based on the methylammonium lead iodide ($CH_3NH_3PBI_3$) perovskite is demonstrated. Such a self-powered PD can operate even with irregular motion such as human finger tapping, which enables it to work without a bulky external power source. In addition, with high-quality $CH_3NH_3PBI_3$ perovskite thin film fabricated with solvent engineering, the PD exhibits an impressive detectivity of 1.22×10^{13} Jones. In the self-powered voltage detection mode, it achieves a large responsivity of up to 79.4 V mW^{-1} cm^{-2} and a voltage response of up to ≈90%. Moreover, as the PD is made of flexible and transparent polymer films, it can operate under bending and functions at 360 Â° of illumination. As a result, the self-powered, flexible, 360 Â° omnidirectional perovskite PD, featuring high detectivity and responsivity along with real-world sensing capability, suggests a new direction for next-generation optical communications, sensing, and imaging applications.

Flexible, portable, and self-powered photodetectors (PDs) are highly desirable for applications in image sensing and optical communications. PDs with high detectivity that can respond to weak optical signals are also especially important for weak light detection, such as ambient light monitoring in smart buildings. Various types of semiconductors, including Si, InGaAs, ZnO, quantum dots, and organic polymers have been extensively explored for use in PDs with varying success. This is because these materials behave differently in term of their responsivity (R), detectivity (D^*), and response time, largely due to their distinct bandgaps, spectral responses, and carrier mobility/diffusion lengths.[1–12]

In the last few years, organometallic halide perovskites have attracted enormous attention in optoelectronic applications due to their outstanding properties, such as strong absorption in the UV–vis wavelengths, long carrier diffusion lengths, and widely tunable bandgaps. Furthermore, polycrystalline and single crystalline perovskite materials could be easily prepared from solution-process at low temperatures on flexible substrates. As a result of these advantages, organometallic halide perovskites have been employed in diverse optoelectronic devices, including solar cells, light-emitting diodes, and PDs.[11,13–20] For example, Dou et al. reported a solution-processed perovskite PD with high detectivity, and Saidamiov et al. demonstrated a PD based on a single crystalline perovskite, which featured longer carrier diffusion lengths than the polycrystalline material.[11,18] These results demonstrate the extraordinary potential of perovskites as active materials in optoelectronic devices.

For self-powered applications, triboelectric nanogenerators (TENGs) have demonstrated promising capabilities in harvesting mechanical energy from motion produced from various sources such as humans, wind, and even water droplets. The advantages of TENGs include a high electrical output, simple design and fabrication, and a rich variety of materials that exhibit the triboelectric effect.[4,21–28] What is more, different types of sensing systems powered by TENGs are being developed, including those that can detect touch, vibrations, UV light, and molecules using low-cost, highly portable, and widely applicable designs.[21,22,29–32] Moreover, sensors based on TENGs are self-powered (i.e., no external power or storage system is needed) and thus are highly favorable for operating in remote areas as well as outdoor applications.

Recently, researchers reported self-powered organometallic halide perovskite PDs driven by TENGs, in which the perovskite served as both the photoresponsive and triboelectric material.[29,30] Unfortunately, the responsivity of these devices has been very limited since the triboelectric property of perovskites is not as good as the state-of-the-art triboelectric materials, such as polydimethylsiloxane (PDMS) and polyimides. Alternatively,

Dr. S.-F. Leung, K.-T. Ho, P.-K. Kung, Dr. V. K. S. Hsiao, Prof. J.-H. He
Computer, Electrical and Mathematical Sciences and Engineering
King Abdullah University of Science and Technology
Thuwal 23955-6900, Kingdom of Saudi Arabia
E-mail: jrhau.he@kaust.edu.sa

Prof. H. N. Alshareef
Physical Sciences and Engineering
King Abdullah University of Science and Technology
Thuwal 23955-6900, Kingdom of Saudi Arabia

Prof. Z. L. Wang
School of Materials Science and Engineering
Georgia Institute of Technology
Atlanta, GA 30332-0245, USA

The ORCID identification number(s) for the author(s) of this article can be found under https://doi.org/10.1002/adma.201704611.

DOI: 10.1002/adma.201704611

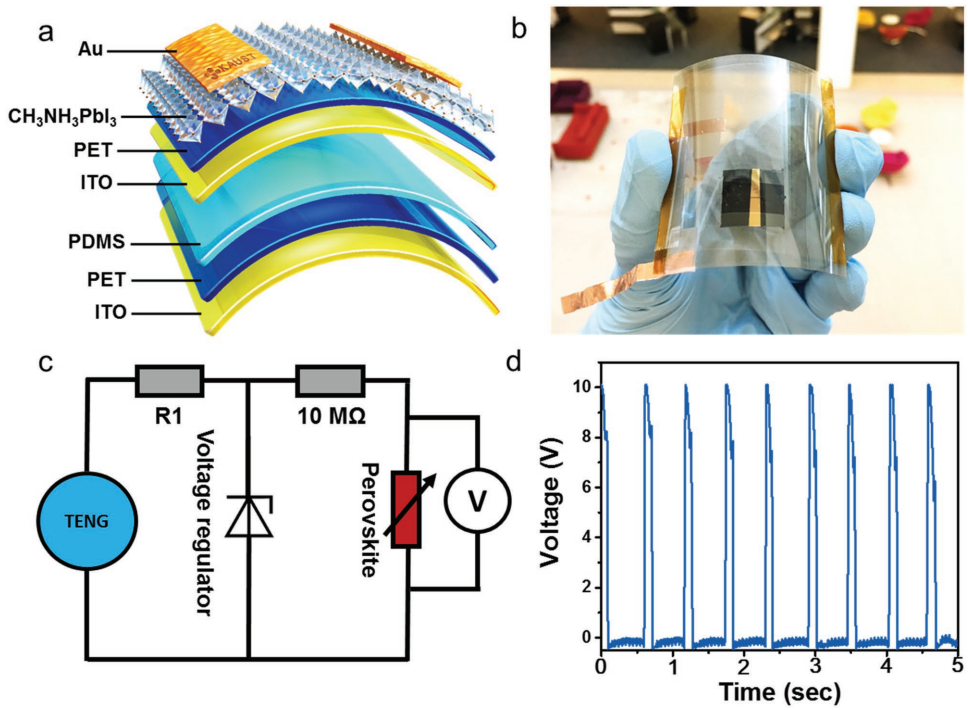

Figure 1. a) Schematic diagram of the self-powered perovskite PD. b) Optical image of the perovskite PD demonstrating its high transparency and flexibility. c) Equivalent circuit diagram of the PD. d) Regulated voltage output of the TENG driven by finger tapping, which corresponds to the voltage spikes.

the PD and TENG components can be separated into two parts of the device in order to achieve better performance, but this design substantially increases the bulkiness of the system, which is not favorable for practical use. Moreover, most TENG-powered PDs are driven by a motion actuator, inconsistencies of which can cause false signals to be detected.

In this work, we demonstrate a self-powered and flexible PD based on the methylammonium lead iodide ($CH_3NH_3PbI_3$) perovskite. Using a voltage regulating circuit, we demonstrate that the TENG-powered PD can perform consistently even with irregular motion, such as human finger tapping, which enables it to work without a bulky external power source and motion actuator. In addition, we were able to fabricate a high-quality $CH_3NH_3PbI_3$ perovskite thin film using solvent engineering, which enables the PD to exhibit an impressive detectivity of 1.22×10^{13} Jones, suggesting applications for the detection of ambient-level light.[11,33] When the device is being self-powered by the TENG, it can achieve a large responsivity of up to 79.4 V mW^{-1} cm^{-2} and a voltage response of up to ≈90% between the highest and the lowest light intensities studied. The importance of resistance matching between the TENG and the perovskite to the voltage response of the PD will be discussed. Moreover, as the PD is made of flexible polymer films, it demonstrates no degradation in device performance after being bent for 1000 times. Because its polymer base is mostly transparent, the PD also functions at 360° of illumination. In field tests done at different lighting conditions, the PD can respond to various light intensities, including ambient light. As a result, the self-powered, flexible, 360° omnidirectional perovskite PD, featuring high detectivity and responsivity along with real-world sensing capability, suggests a new direction for next-generation optical communications, sensing and imaging applications.

Figure 1a shows the schematic of the flexible, self-powered perovskite PD, which was built on two polymer films. The detailed fabrication process can be found in the Experimental Section. In brief, we first prepared two polymer films composed of commercial indium-doped tin-oxide/polyethylene terephthalate (ITO/PET) and PDMS-coated PET. We then spin-coated a 1.5 × 1.5 cm^2 area of $CH_3NH_3PbI_3$ on the PET side of the ITO/PET sheet using solvent engineering (details discussed later) to serve as the photoabsorptive layer.[15] Two gold electrodes spaced 100 µm apart were then deposited on the perovskite layer by e-beam evaporation. A top-view scanning electron microscopy (SEM) image of the resulting device can be seen in Figure S1 of the Supporting Information. For the other TENG electrode, a 200 nm thick layer of ITO was deposited on the PET side of the PDMS/PET film using DC magnetron sputtering. We bonded the two films together using Kapton tape so that the ITO side of the ITO/PET film faced the PDMS side of the PDMS/PET. A 5 mm gap was left between the two polymer films (Figure S2, Supporting Information), which enabled us to harness the triboelectrification effect generated between the ITO and the PDMS as the device was physically manipulated by finger tapping. Figure 1b shows an optical image of the self-powered perovskite PD, demonstrating its high transparency and flexibility. A detailed schematic of the device indicating the multiple layers and configuration can be found in Figure S3 of the Supporting Information. The self-powered PD was completed by connecting the two ITO terminals of the TENG to the

gold electrodes of the PD. The equivalent circuit diagram is shown in Figure 1c.

When the photoabsorptive perovskite is illuminated by light, the resistivity will decrease due to the photogenerated carriers. Therefore, the electric potential difference across the perovskite decreases when the voltage generated by the TENG is divided by the perovskite and a 10 MΩ resistor. Utilizing this principle, the intensity of the incident light can be detected by monitoring the voltage across the perovskite. It is worth noting that the voltage output of the TENG is modulated by a regulating circuit containing a resistor (R1 in Figure 1c) and a Zener diode, which enables the self-powered PD to function consistently and quantitatively even as it is powered by irregular motion, thus circumventing the need for a bulky motion actuator. Figure 1d demonstrates the resulting highly regulated voltage output of the TENG (the current output can be seen in Figure S4, Supporting Information). This regulated voltage output is especially crucial for the PD application because the detected voltage should solely depend on the intensity of the incident light.

To quantitatively characterize the $CH_3NH_3PbI_3$ perovskite PD, we measured its current–voltage (I–V) performance using a 1 V bias at different light intensities (10 μW cm^{-2} to 100 mW cm^{-2}) by attenuating 1 sun (100 mW cm^{-2}) simulated sunlight using neutral density filters (**Figure 2**a). The photocurrent increases with light intensity as expected due to the increased number of photogenerated carriers in response to the higher photon flux. Figure 2b shows the photocurrent of the perovskite PD under weak light intensity, as low as 10 μW cm^{-2}. Even at this low intensity, we note that the resulting photocurrent is still twofold higher than that under dark conditions. In term of the photocurrent against time, we have measured the photocurrent of the PD (at 10 mW cm^{-2}, 1 V bias) at day 1, 3, 5, and 10, respectively, and the data are shown in Figure S5 of the Supporting Information. It can be seen that the perovskite behave as other normal $CH_3NH_3PbI_3$ perovskites in term of the chemical stability. It is also determined that the response time of the perovskite PD was less than 80 ms, which is the detection limit of our setup (Figure S6, Supporting Information).

Detectivity (D^*) is an important parameter that indicates the ability of a PD to measure weak optical signals. D^* is given by Equation (1)

$$D^* = \frac{R}{\sqrt{2qI_{\text{Dark}}}} \tag{1}$$

in which R is the responsivity, I_{dark} is the dark current, and q is the elementary charge. In addition to the unique self-powered capability of the device, our perovskite PD exhibits a detectivity as high as 1.22×10^{13} Jones in the conventional current detection mode, which is comparable to the performance of state-of-the-art PDs based on Si (the most common PD material) and among the highest when compared with other organometallic halide perovskites based PDs, as summarized in Table S1 of Supporting Information.[1,11,34–38] Noted that we did not calculate the detectivity in the self-powered operation mode due to the insufficient current output by the TENG. We attribute this high detectivity to the strong optical absorption

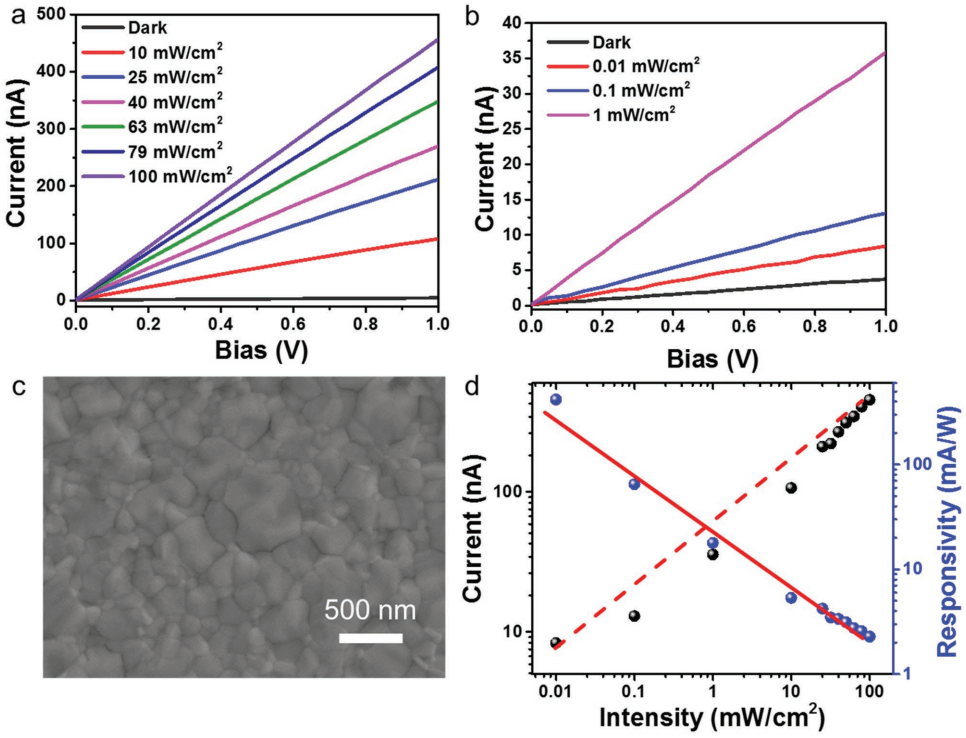

Figure 2. a) I–V curves of the perovskite PD measured under various intensities of light, including b) weak light conditions in conventional current detection mode. c) Top-view SEM image of the high quality $CH_3NH_3PbI_3$ thin film processed with solvent engineering. d) Photocurrent and responsivity of the perovskite PD under various intensities of light.

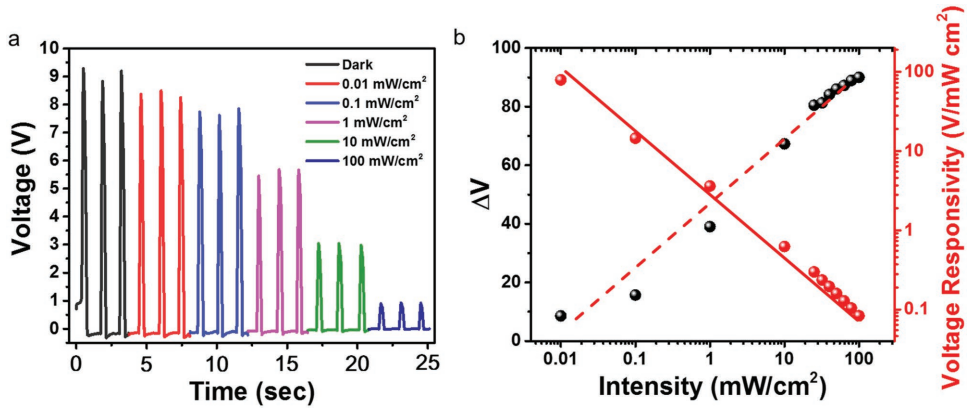

Figure 3. a) The PD device voltage measured across the perovskite under various intensities of light in voltage detection mode. b) The change in the measured voltage (ΔV) and voltage responsivity of the device at different light intensities.

of $CH_3NH_3PbI_3$ and the high quality perovskite film obtained by solvent engineering.[15] This process involved the drop-by-drop addition of toluene to the $CH_3NH_3PbI_3$ precursor solution while spin-coating in order to form an intermediate phase that prevents rapid reaction between the CH_3NH_3I and the PbI_2. As a result, highly dense and uniform perovskite thin film is formed, which efficiently suppress photogenerated carrier recombination. More details about perovskite film processed by solvent engineering can be found in the Supporting Information. The successful synthesis of this high quality perovskite film can be seen from the SEM shown in Figure 2c. In addition, AFM results in Figure S7 of the Supporting Information agree with the SEM results that the solvent engineering can result in smoother perovskite layer with better coverage. Furthermore, from the XRD data shown in Figure S8 of the Supporting Information, we could recognize the decrease of PBI_2's characteristic peak and the enhanced intensity of perovskite's characteristic peak. This suggests that the solvent engineering during spin-coating can significantly improve the crystallinity of perovskites.

Next, we characterized the PD photoresponse and responsivity (R) both in conventional current detection mode (by applying a bias across the perovskite) and in self-powered voltage detection mode. Figure 2d demonstrates the photocurrent and responsivity of the PD under different light intensities.[39,40] The responsivity of the device, indicating how efficient the detector responds to the optical signal, is calculated by Equation (2)

$$R = \frac{I_{ph}}{P_{light}}, \tag{2}$$

in which I_{ph} is the photocurrent and P_{light} is the power of the incident light. Based on this equation, we determined that the perovskite PD achieved a responsivity as high as 0.418 A W^{-1} at 10 μW cm^{-2}. It is worth noting that this value is not the highest ever reported for perovskite PDs because the resistance of the PD in this work has been intentionally increased by adjusting the channel width in order to accommodate the internal resistance of the TENG and maximize the sensitivity in the self-powered voltage detection mode. The detailed circuit diagram to explain this can be seen in Figure S9 of the Supporting Information.[11]

In self-powered voltage detection mode, the perovskite PD is connected in series with a 10 MΩ resistor at the output of the TENG. The perovskite acts as a variable resistor with its resistance being modulated by the incident light intensity. In fact, the TENG can be regarded as a battery with very high internal resistance. Thus, if the resistance of the perovskite PD is too low, the electric potential drop at the perovskite would be too small or negligible. Accordingly, we optimized the resistance of the perovskite PD in order to maximize the response in the self-powered voltage detection mode.

Figure 3a shows the measured voltage at the perovskite under various light intensities. The voltage drop at the perovskite decreases with light intensity because the resistance is reduced by photogenerated carriers. To evaluate the performance of the PD in voltage detection mode, we measured the change in voltage (ΔV) and voltage responsivity, which are defined as $\frac{(V_{Dark}-V)}{V_{Dark}}\times 100\%$ and $\frac{V_{Dark}-V}{P_{Light}}$, respectively (Figure 3b). The results demonstrate that the PD can achieve a large ΔV of up to ≈90% at an incident light intensity of 100 mW cm^{-2} compared to in the dark, which demonstrates the excellent sensitivity of the self-powered perovskite PD. This impressive voltage response can be attributed to the optimized resistance matching between the TENG and the perovskite. Moreover, the steepest ΔV occurred between light intensities of 10 μW cm^{-2} to 25 mW cm^{-2}, which suggests that the perovskite PD is more sensitive under weak light conditions. Meanwhile, the PD reaches a maximum voltage responsivity of 79.4 V mW^{-1} cm^{-2}, which is a remarkably high value that benefits from the large and stable voltage output of the TENG. Additionally, it is worth mentioning that the TENG used in this work was regulated at 10 V, which is a relatively small voltage and we believe that this responsivity could be even further enhanced using TENGs featuring higher voltage outputs, as has been reported extensively.[22,28]

Another advantage of the TENG-powered perovskite PD is its flexibility during operation. This means it can be fabricated on either rigid or flexible substrates. **Figure 4**a shows a photograph of the PD fitted on a curved surface, which demonstrates its potential to be used in real-world applications, such as ambient light monitoring in smart buildings. Additionally, the PD shows excellent performance stability while being repeatedly bent.

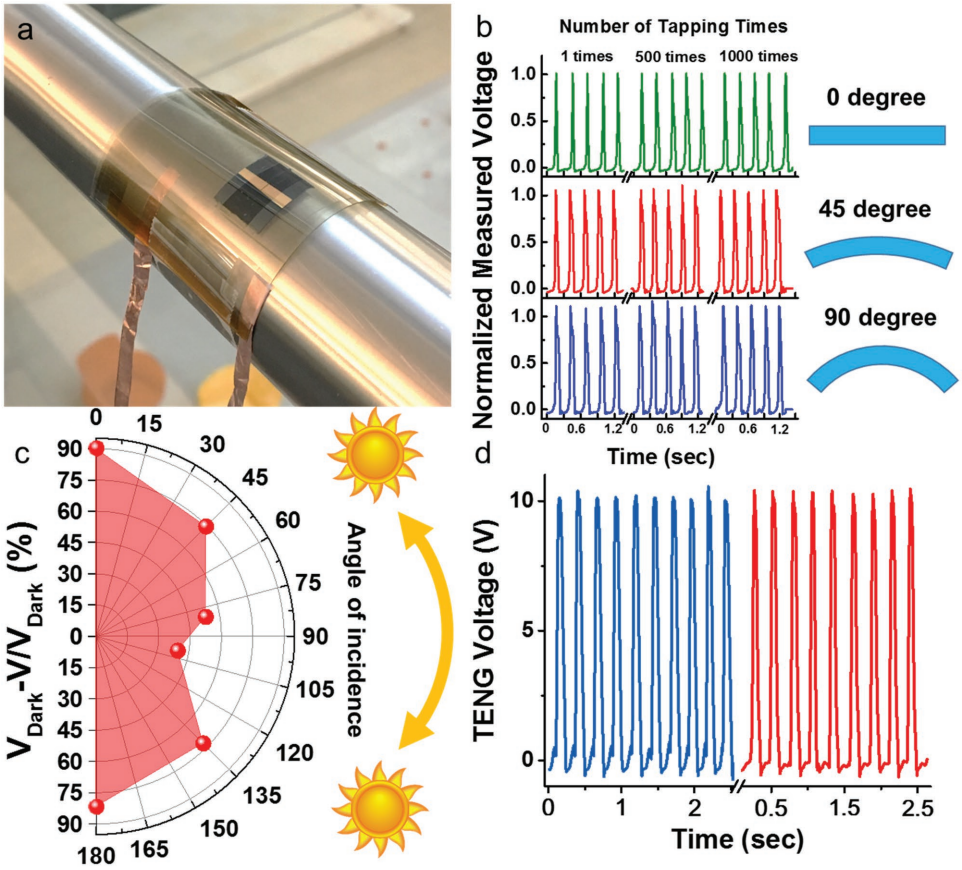

Figure 4. a) Photograph of a perovskite PD attached to a curved surface. b) The self-powered perovskite PD features stable performance upon repeated bending at various angles of curvature. c) ΔV at various angles of incident light. d) The TENG output by two different people, demonstrating the highly regulated TENG voltage output as a result of the regulating circuit.

Figure 4b displays the normalized voltage of the self-powered PDs during prolonged operation at three different bending angles, including 0° (nonbended), 45°, and 90° under 1 sun illumination. For each bending angle, we measured the voltage after the PD had been powered by finger tapping the device 1, 500, and 1000 times. A detailed procedure for this study can be found in the Experimental Section. The performance of the PD was very stable at these different angles of curvature, as the voltage remained unchanged even while the device was powered by 1000 repetitions of finger taping. Meanwhile, we observed the normalized voltages slightly increased when the PD was bent at 45° and 90°, which implies that the resistance of the perovskite increased slightly in both cases. This can be explained by the appearance of microcracks as the device was bent (Figure S10, Supporting Information). These microcracks hinder the collection of photogenerated charge carriers, resulting in a larger voltage drop in the perovskite active layer.

Since the PD was fabricated with transparent materials, including PDMS, PET, and ITO, the device can function whether it is illuminated from the top or bottom. This can be seen from Figure 4c, which demonstrates a plot of ΔV under various angles of incidence, in which 0° refers to illumination from the top-side of the device and 180° refers to illumination from beneath the PD. When the angle of incidence was increased to 45° and 80°, ΔV was reduced due to a stronger surface reflection, which results in less optical absorption by the perovskite layer. Moreover, ΔV for the illumination from the backside of the PD was slightly lower than that for illumination from the top, which can be explained by the parasitic absorption of the ITO. Overall, these results demonstrate that the PD features omnidirectional light-harvesting capabilities, and good durability under various bending conditions.

Additionally, conventional TENG-powered devices require a motion actuator to power the system during operation. However, the voltage output by the TENG might be variable, depending on how the surrounding conditions influence the actuator's motion, which can affect the accuracy of photodetection. The PD reported in this work utilizes a voltage regulating circuit to ensure the detected voltage only depends on the light intensity, rather than the mechanical pressure being applied to the TENG. Furthermore, this design allows the PD to function properly even under irregular mechanical motions (for example, in this work we powered the device by finger tapping), which greatly enhances the versatility of the system. Figure 4d shows two sets of the TENG output (displayed in blue and red) when operated by two different people. The results are highly consistent, which is important for ensuring the accuracy in the self-powered voltage detection mode.

Besides systematically characterizing the PD in the lab, we also performed field tests to study the device performance under

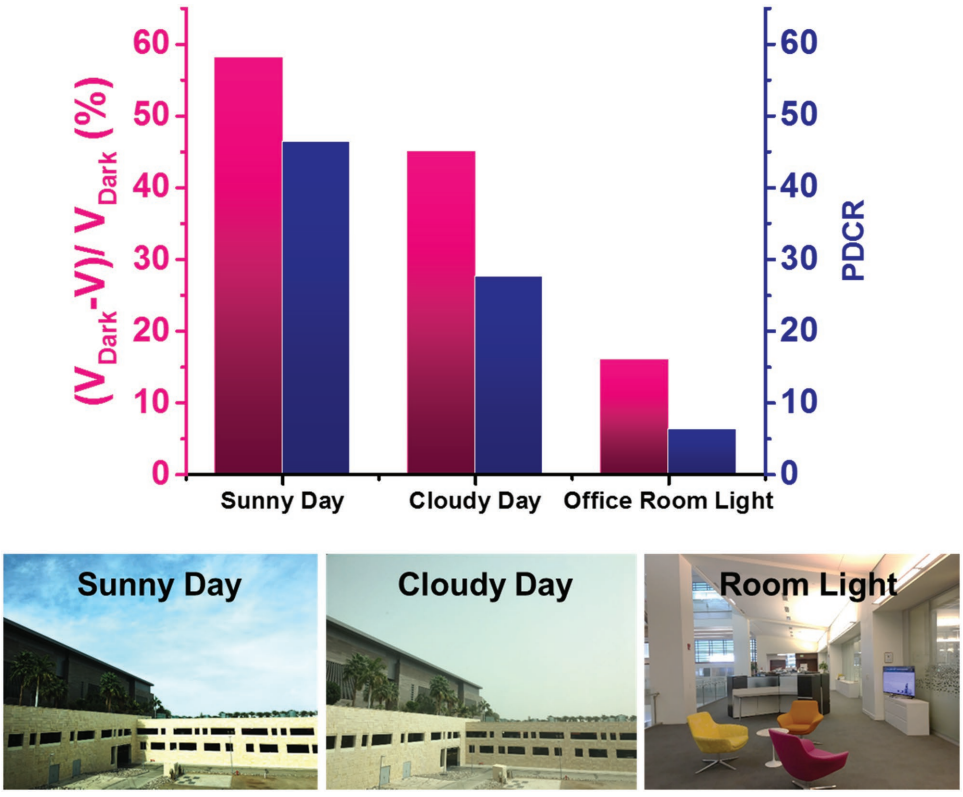

Figure 5. The ΔV and PDCR of the perovskite PD under sunny, cloudy, and room lighting conditions. The sunny and cloudy days occurred at N 22°18′30″ and E 39°06′20″ at 11:00 on March 16th, 2017 and 15:00 on March 21st, 2017, respectively.

different environments, including sunny, cloudy, and indoor lighting conditions. A detailed description of the field tests can be found in the Experimental Section. **Figure 5** presents the photo-to-dark current ratio (PDCR, defined as $\frac{(I_{Light}-I_{Dark})}{I_{Dark}}$) and ΔV of the PD, which represent the results from the conventional current detection mode and the self-powered voltage-detection mode, respectively, both of which feature the same trend. Notably, the PD exhibited a ΔV of 58%, 45%, and 16% on sunny, cloudy, and room lighting conditions, respectively, which shows the PD can clearly distinguish between different levels of light. We ascribe this performance to the optimized resistance matching between the perovskite PD and the TENG. These results demonstrate the strong functionality and sensitivity of the self-powered PD in real-world environments.

In conclusion, we have demonstrated a self-powered, flexible and transparent organometallic halide perovskite PD. The photodetector is versatile and exhibits stable prolonged operation under different bending angles, different environments, and varying incident angles of light. The PD also exhibits an impressive detectivity of 1.22×10^{13} Jones in the current detection mode, and a large responsivity of up to 79.4 V mW^{-1} cm^{-2} in self-powered voltage detection mode. These results were made possible through the use of a high quality $CH_3NH_3PbI_3$ thin film, which we achieved using solvent engineering. In addition, the PD demonstrates a voltage response of up to ≈90% between the highest and the lowest light intensities studied, which can be attributed to the optimized resistance matching between the TENG and the PD. More importantly, with the voltage regulating circuit, the self-powered PD functions with regular precision even as irregular mechanical forces are applied, such as by human finger tapping, all without the aid of a bulky external power system or motion actuator. These results demonstrate a simple and promising approach for developing a flexible and self-powered sensing system for applications such as smart textiles and smart buildings.

Experimental Section

Fabrication of the Perovskite PD: A 5.5 cm × 5 cm commercial ITO/PET film (Sigma-Aldrich) with resistivity of 100 Ω sq^{-1} area and a 5 cm × 5 cm PDMS-coated PET film (Gel-Pak, PF film) was prepared and cleaned with acetone, isopropanol, and deionized water. A 1:1 molar ratio of CH_3NH_3I (Dyesol) and PbI_2 (99.9985%, Alfa Aesar) were dissolved in a solution composed of gamma-butyrolactone and dimethyl sulfoxide (Sigma-Aldrich, ACS reagent grade) (3:2, v/v) at 50 °C for 24 h. The perovskite solution was filtered (PTFE filter, 0.45 µm pore size, Fisherbrand) and then spin-coated onto a 1.5 × 1.5 cm^2 area as defined by Kapton tape on the PET side of the ITO/PET film. Spin-coating involved two stages at 5000 and 1000 rpm for 20 and 10 s, respectively. Approximately 50 µL of toluene was added drop-by-drop during the second stage of spin-coating to form an intermediate phase that prevented the CH_3NH_3I and PbI_2 reagents from reacting too quickly, thus enabling a uniform $CH_3NH_3PbI_3$ film to be deposited onto the PET surface. Two 40 nm thick gold electrodes were then deposited 100 µm apart on top of the perovskite layer by e-beam evaporation. For the other side of the TENG electrode, a 200 nm thick layer of ITO was deposited on the PET side of the PDMS-coated PET film by DC magnetron sputtering. Finally, the two films were bonded together with the ITO side of the ITO/PET film facing the PDMS side

of the other film using Kapton tape. A small gap of about 5 mm was left between the two films since one film was slightly longer than the other as shown in Figure S2 of the Supporting Information.

Voltage Regulating Circuits: The voltage regulating circuits which limit the output voltage of the TENGs consist of a Zener diode and resistor. Zener diode allows a wide range of currents when a reverse voltage exceeds a threshold value which called Zener voltage. In this work, a Zener diode with Zener voltage of 10 V has been chosen and connected it at the output of the TENGs. As a result, the voltage of the TENGs is regulated at 10 V.

Device Characterization and Field Testing Conditions: SEM characterization was performed using an FEI Zeiss Merlin field emission SEM. An Enlitech 350 W Xe lamp with an AM 1.5G filter was used for 1 sun simulated illumination. A Thorlab NDK01 ND filter kit was used to produce incident light at various intensities, from 10 μW cm^{-2} to 100 mW cm^{-2}. Note that 10 μW cm^{-2} is the lowest intensity can be produced by this ND filter set. For *I–V* characterization in conventional current detection mode, a Keithley 2420 source meter was used to measure the current flow across the perovskite with 1 V DC bias. In the self-powered voltage detection mode, a National Instruments BNC-2120 board with homemade data acquisition software was used to measure the voltages across the perovskite while the PD was being powered by the TENG. D^* and R were calculated by Equations (1) and (2). For the bending and durability tests, the voltage was measured across the perovskite PD under bending angles of 0°, 45°, and 90°. At each bending angle, the voltage was measured after the self-powered PD had been powered by finger tapping for 1, 500, and 1000 times. The voltages measured were normalized to indicate the changes upon bending and prolonged operation. For the conditions of the field test, the sunny and cloudy days occurred at N 22°18′30″ and E 39°06′20″ at 11:00 on March 16th, 2017 and 15:00 on March 21st, 2017, respectively.

Supporting Information

Supporting Information is available from the Wiley Online Library or from the author.

Acknowledgements

This work was financially supported by the King Abdullah University of Science and Technology (KAUST) Office of Sponsored Research (OSR-2016-CRG5-3005), KAUST Sensor Initiative, KAUST Solar Center, and KAUST baseline funding.

Conflict of Interest

The authors declare no conflict of interest.

Keywords

flexible electronics, organometallic halide perovskites, photodetectors, self-powered electronics, solvent engineering, triboelectric nanogenerators

Received: August 14, 2017
Revised: November 2, 2017
Published online:

[1] X. Gong, M. Tong, Y. Xia, W. Cai, J. S. Moon, Y. Cao, G. Yu, C.-L. Shieh, B. Nilsson, A. J. Heeger, *Science* **2009**, *325*, 1665.
[2] G. Konstantatos, I. Howard, A. Fischer, S. Hoogland, J. Clifford, E. Klem, L. Levina, E. H. Sargent, *Nature* **2006**, *442*, 180.
[3] B. Levine, C. Bethea, G. Hasnain, V. Shen, E. Pelve, R. Abbott, S. Hsieh, *Appl. Phys. Lett.* **1990**, *56*, 851.
[4] S. Liang, H. Sheng, Y. Liu, Z. Huo, Y. Lu, H. Shen, *J. Cryst. Growth* **2001**, *225*, 110.
[5] S. A. McDonald, G. Konstantatos, S. Zhang, P. W. Cyr, E. J. Klem, L. Levina, E. H. Sargent, *Nat. Mater.* **2005**, *4*, 138.
[6] T. Mueller, F. Xia, P. Avouris, *Nat. Photonics* **2010**, *4*, 297.
[7] C. Soci, A. Zhang, B. Xiang, S. A. Dayeh, D. Aplin, J. Park, X. Bao, Y.-H. Lo, D. Wang, *Nano Lett.* **2007**, *7*, 1003.
[8] J. B. Soole, H. Schumacher, *IEEE J. Quantum Electron.* **1991**, *27*, 737.
[9] C.-P. Lee, C.-A. Lin, T.-C. Wei, M.-L. Tsai, Y. Meng, C.-T. Li, K.-C. Ho, C.-I. Wu, S.-P. Lau, J.-H. He, *Nano Energy* **2015**, *18*, 109.
[10] M.-L. Tsai, M.-Y. Li, Y. Shi, L.-J. Chen, L.-J. Li, J.-H. He, *Nanoscale Horiz.* **2017**, *2*, 37.
[11] L. Dou, Y. M. Yang, J. You, Z. Hong, W.-H. Chang, G. Li, Y. Yang, *Nat. Commun.* **2014**, *5*, 5404.
[12] S. Xu, Y. Qin, C. Xu, Y. Wei, R. Yang, Z. L. Wang, *Nat. Nanotechnol.* **2010**, *5*, 366.
[13] Y. Fang, J. Huang, *Adv. Mater.* **2015**, *27*, 2804.
[14] X. Hu, X. Zhang, L. Liang, J. Bao, S. Li, W. Yang, Y. Xie, *Adv. Funct. Mater.* **2014**, *24*, 7373.
[15] N. J. Jeon, J. H. Noh, Y. C. Kim, W. S. Yang, S. Ryu, S. I. Seok, *Nat. Mater.* **2014**, *13*, 897.
[16] Y. H. Kim, H. Cho, J. H. Heo, T. S. Kim, N. Myoung, C. L. Lee, S. H. Im, T. W. Lee, *Adv. Mater.* **2015**, *27*, 1248.
[17] M. Liu, M. B. Johnston, H. J. Snaith, *Nature* **2013**, *501*, 395.
[18] M. I. Saidaminov, V. Adinolfi, R. Comin, A. L. Abdelhady, W. Peng, I. Dursun, M. Yuan, S. Hoogland, E. H. Sargent, O. M. Bakr, *Nat. Commun.* **2015**, *6*, 8724.
[19] Z.-K. Tan, R. S. Moghaddam, M. L. Lai, P. Docampo, R. Higler, F. Deschler, M. Price, A. Sadhanala, L. M. Pazos, D. Credgington, *Nat. Nanotechnol.* **2014**, *9*, 687.
[20] T.-C. Wei, H.-P. Wang, C.-H. Lin, Y.-H. Hsieh, Y.-H. Chu, J.-H. He, *Adv. Mater.* **2017**, *29*, 1701789.
[21] Z. L. Wang, J. Chen, L. Lin, *Energy Environ. Sci.* **2015**, *8*, 2250.
[22] Z. L. Wang, *ACS Nano* **2013**, *7*, 9533.
[23] Z. H. Lin, G. Cheng, S. Lee, K. C. Pradel, Z. L. Wang, *Adv. Mater.* **2014**, *26*, 4690.
[24] S. Lee, S. H. Bae, L. Lin, Y. Yang, C. Park, S. W. Kim, S. N. Cha, H. Kim, Y. J. Park, Z. L. Wang, *Adv. Funct. Mater.* **2013**, *23*, 2445.
[25] P.-K. Yang, Z.-H. Lin, K. C. Pradel, L. Lin, X. Li, X. Wen, J.-H. He, Z. L. Wang, *ACS Nano* **2015**, *9*, 901.
[26] P. K. Yang, L. Lin, F. Yi, X. Li, K. C. Pradel, Y. Zi, C. I. Wu, H. He Jr., Y. Zhang, Z. L. Wang, *Adv. Mater.* **2015**, *27*, 3817.
[27] P. Bai, G. Zhu, Z.-H. Lin, Q. Jing, J. Chen, G. Zhang, J. Ma, Z. L. Wang, *ACS Nano* **2013**, *7*, 3713.
[28] G. Zhu, Z.-H. Lin, Q. Jing, P. Bai, C. Pan, Y. Yang, Y. Zhou, Z. L. Wang, *Nano Lett.* **2013**, *13*, 847.
[29] L. Su, Z. Zhao, H. Li, Y. Wang, S. Kuang, G. Cao, Z. L. Wang, G. Zhu, *J. Mater. Chem. C* **2016**, *4*, 10395.
[30] L. Su, Z. X. Zhao, H. Y. Li, J. Yuan, Z. L. Wang, G. Z. Cao, G. Zhu, *ACS Nano* **2015**, *9*, 11310.
[31] H. Fang, Q. Li, J. Ding, N. Li, H. Tian, L. Zhang, T. Ren, J. Dai, L. Wang, Q. Yan, *J. Mater. Chem. C* **2016**, *4*, 630.
[32] Z. H. Lin, G. Cheng, Y. Yang, Y. S. Zhou, S. Lee, Z. L. Wang, *Adv. Funct. Mater.* **2014**, *24*, 2810.
[33] M.-L. Tsai, D.-S. Tsai, L. Tang, L.-J. Chen, S. P. Lau, J.-H. He, *ACS Nano* **2017**, *11*, 4564.
[34] L. Wang, J. Jie, Z. Shao, Q. Zhang, X. Zhang, Y. Wang, Z. Sun, S. T. Lee, *Adv. Funct. Mater.* **2015**, *25*, 2910.

[35] X. Li, M. Zhu, M. Du, Z. Lv, L. Zhang, Y. Li, Y. Yang, T. Yang, X. Li, K. Wang, *Small* **2016**, *12*, 595.
[36] H. Zhang, S. Jenatsch, J. De Jonghe, F. Nüesch, R. Steim, A. C. Véron, R. Hany, *Sci. Rep.* **2015**, *5*, 9439.
[37] M. Kielar, O. Dhez, G. Pecastaings, A. Curutchet, L. Hirsch, *Sci. Rep.* **2016**, *6*, 39201.
[38] H. Zhang, X. Zhang, C. Liu, S.-T. Lee, J. Jie, *ACS Nano* **2016**, *10*, 5113.
[39] J. R. D. Retamal, C.-Y. Chen, D.-H. Lien, M. R. Huang, C.-A. Lin, C.-P. Liu, J.-H. He, *ACS Photonics* **2014**, *1*, 354.
[40] D.-S. Tsai, D.-H. Lien, M.-L. Tsai, S.-H. Su, K.-M. Chen, J.-J. Ke, Y.-C. Yu, L.-J. Li, J.-H. He, *IEEE J. Quantum Electron.* **2014**, *20*, 30.